Structure of the Carboxy-Terminal Fragment of the Apo-Biotin Carboxyl Carrier Subunit of *Escherichia coli* Acetyl-CoA Carboxylase†

Xiang Yao,‡,§ Dong Wei,‡ Cylburn Soden, Jr.,‡,§ Michael F. Summers,*,‡,§ and Dorothy Beckett*,‡

Department of Chemistry and Biochemistry and Howard Hughes Medical Institute, University of Maryland Baltimore County, 1000 Hilltop Circle, Baltimore, Maryland 21250

Received June 23, 1997; Revised Manuscript Received September 19, 1997⊗

ABSTRACT: The biotin carboxyl carrier protein (BCCP) is a subunit of acetyl-CoA carboxylase, a biotin-dependent enzyme that catalyzes the first committed step of fatty acid biosynthesis. In its functional cycle the biotin carboxyl carrier protein engages in heterologous protein−protein interactions with three distinct partners, depending on its state of posttranslational modification. Apo-BCCP interacts specifically with the biotin holoenzyme synthetase, BirA, which results in the posttranslational attachment of biotin to an essential lysine residue on BCCP. Holo-BCCP then interacts with the biotin carboxylase subunit, which leads to the addition of the carboxylate group of bicarbonate to biotin. Finally, the carboxybiotinylated form of BCCP interacts with transcarboxylase in the conversion of acetyl-CoA to malonyl-CoA. The determinants of protein−protein interaction specificity in this system are unknown. One hypothesis is that posttranslational modification of BCCP may result in conformational changes that regulate specific protein−protein interactions. To test this hypothesis, we have determined the NMR solution structure of the unbiotinylated form of an 87 residue C-terminal domain fragment of BCCP (apoBCCP87) from *Escherichia coli* acetyl-CoA carboxylase and compared this structure with the high-resolution structure of the biotinylated form that was recently solved by X-ray crystallographic techniques. Although the overall folding of the two proteins is highly similar, small structural differences are apparent for residues of the biotin-binding loop that may be important for mediating specific protein−protein interactions.

The biotin-dependent carboxylases are a class of enzymes found in organisms across the evolutionary spectrum. These enzymes catalyze reactions of fundamental metabolic significance involving transfer of carboxylate to a variety of substrates (Knowles, 1989). In these two step reactions the carboxyl moiety of a donor, usually bicarbonate, is first incorporated into the biotin cofactor in the enzyme and subsequently transferred to a second substrate. An example of this class of reactions is the transfer of CO_2 from bicarbonate to acetyl-CoA to produce malonyl-CoA, the reaction that constitutes the first committed step in fatty acid biosynthesis. This reaction, which is shown schematically in Figure 1, is catalyzed by the enzyme acetyl-CoA carboxylase.

Like all biotin-dependent carboxylases, acetyl-CoA carboxylase requires three functional components to catalyze the conversion of acetyl-CoA to malonyl-CoA (Alberts & Vagelos, 1972). These include the biotin carboxyl carrier, which carries the biotin moiety; biotin carboxylase, which catalyzes the initial carboxylation of the biotin moiety; and transcarboxylase, which catalyzes the transfer of the CO_2 moiety from biotin to acetyl-CoA (Alberts & Vagelos, 1972). In the *Escherichia coli* enzyme these three activities are encoded in distinct polypeptide components. The biotin carboxyl carrier protein is a polypeptide of approximately 17 kDa (Li & Cronan, 1992a) and the biotin carboxylase activity is encoded by a polypeptide with a molecular mass of 50 kDa (Li & Cronan, 1992b; Dimroth et al., 1970). The transcarboxylase activity is encoded in two polypeptide chains that are 30 and 35 kDa (Guchhait et al., 1974; Li & Cronan, 1992b). The stoichiometry of the polypeptide chains in the assembled enzyme is not known.

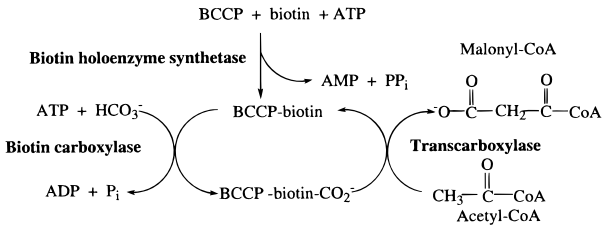

FIGURE 1: Schematic representation of the three heterologous protein−protein interactions in which the biotin carboxyl carrier protein (BCCP) participates in the functional cycle of acetyl-CoA carboxylase. The BCCP subunit is first posttranslationally modified in the reaction catalyzed by the biotin holoenzyme synthetase. Interaction of the biotinylated BCCP with biotin carboxylase results in carboxylation of the biotin moiety. Finally, interaction of carboxybiotinylated BCCP with transcarboxylase results in transfer of the carboxylate group to acetyl-CoA to yield malonyl-CoA.

In the functional cycle of acetyl-CoA carboxylase, the biotin carboxyl carrier protein (BCCP)[1] participates in three

† This work was supported by NIH Grant GM 46511 (D.B.).

* To whom correspondence should be addressed. M.F.S.: Phone (410) 455-2527; E-mail summers@hhmi.umbc.edu. D.B.: Phone (410) 455-2512; E-mail beckett@umbc7.umbc.edu.

‡ Department of Chemistry and Biochemistry.

§ Howard Hughes Medical Institute.

⊗ Abstract published in *Advance ACS Abstracts,* November 15, 1997.

[1] Abbreviations: BCCP, biotin carboxyl carrier protein; BHS, biotin holoenzyme synthetase; 2D, two-dimensional; 3D, three-dimensional; HSQC, heteronuclear single quantum coherence spectroscopy; NOESY, nuclear Overhauser effect spectroscopy; TOCSY, total correlation spectroscopy; HOHAHA, homonuclear Hartmann−Hahn spectroscopy; NOE, nuclear Overhauser effect; ROESY, rotating Overhauser effect spectroscopy; T_1, longitudinal relaxation time constants; T_2, transverse relaxation time constants; S^2, generalized order parameters; τ_e, internal correlation times; R_{ex}, chemical exchange terms; MALDI-TOFMS, matrix-assisted laser desorption ionization time of flight mass spectrometry.

S0006-2960(97)01485-2 CCC: $14.00

heterologous protein−protein interactions. First, it serves as the substrate in the biotin ligation reaction catalyzed by the biotin holoenzyme synthetase (BHS), in which the cofactor is linked to a specific lysine residue of apoBCCP. Second, in its biotinylated form, holoBCCP interacts with the biotin carboxylase subunit in the incorporation of CO_2 into the ureido group of the biotin ring system. Finally the carboxylated holo carrier protein interacts with transcarboxylase in the reaction in which the CO_2 moiety is transferred to acetyl-CoA to yield malonyl-CoA.

Selective BHS-catalyzed posttranslational addition of biotin to a single lysine residue of apoBCCP occurs in two steps, in which the biotin is first activated via formation of an adenylate derivative and is then transferred to the ϵ-amino group of the lysine residue (Lane et al., 1964). The biotin ligation reaction is highly specific and in *E. coli* only the BCCP subunit of acetyl-CoA carboxylase is biotinylated (Fall, 1979). Elucidation of the determinants of specificity in the biotinylation of apoBCCP as well as the structural basis for interaction of holoBCCP with the biotin carboxylase and transcarboxylase requires knowledge of the three-dimensional structures of all of the participants in these reactions. Some progress has already been made in this effort. The structures of the *E. coli* biotin holoenzyme synthetase (BirA) and the biotin carboxylase have been solved by X-ray crystallographic techniques (Wilson et al., 1992; Waldrop et al., 1994). More recently, the crystal structure of the biotinylated (or holo) form of a carboxy-terminal domain fragment of BCCP (BCCPsc) was determined at 1.8 Å resolution (Athappilly & Hendrickson, 1995).

The apo form of BCCP is the significant species in the biotin ligation reaction and its structure is, therefore, relevant to elucidating structure−function relationships in specific biotinylation catalyzed by the BHS. It is, furthermore, of interest to determine if any structural changes occur as a consequence of biotinylation of the subunit. Biotinyl domains have been shown to bear sequence and structural homology to the lipoyl domains of lipoic acid-dependent enzymes (Lim et al., 1988; Brocklehurst & Perham, 1993; Dardel et al., 1993). In this regard, high-resolution structures of the lipoyl domains from *Bacillus stearothermophilus* and *E. coli* pyruvate dehydrogenase multienzyme complexes have been determined by NMR spectroscopy (Dardel et al., 1993; Green et al., 1995), and the structure of the lipoate-containing or H-protein of the glycine decarboxylase from pea leaves has been solved by X-ray crystallography (Pares et al., 1994). Comparison of 2D NMR spectra obtained from samples of the lipoated and unlipoated forms of the domain from the *B. stearothermophilus* pyruvate dehydrogenase led to the conclusion that no structural changes occur upon conversion of the apolipoyl domain to the holo form (Dardel et al., 1991). Unfortunately, three-dimensional structural information is only available for the unlipoated form of the domain (Dardel et al., 1993). There is, furthermore, no system for which both structures of the lipoated and unlipoated forms of any lipoyl domain are available.

In this work we have utilized multidimensional nuclear magnetic resonance spectroscopy to determine a high-resolution three-dimensional structure of the unbiotinylated form of an 87 residue C-terminal domain fragment of the biotin carboxyl carrier protein from *E. coli* acetyl-CoA carboxylase. The structure of the apoprotein is very similar to that of the holoprotein, solved by X-ray crystallographic techniques, with small differences observed in the β turn that contains the lysine residue that is modified in the biotin ligation reaction. (Athappilly & Hendrickson, 1995). The backbone dynamics of the protein, determined by ^{15}N relaxation NMR spectroscopy, indicate that in the absence of biotin modification there is significant conformational flexibility in the biocytin-containing loop, as well as the "protruding thumb" with which the biotin moiety is observed to interact in the holoprotein.

MATERIALS AND METHODS

Protein Expression, Purification, and Characterization. ApoBCCP87 was overexpressed from plasmid pTM53 in *E. coli* strain BL21λDE3, generously provided by Dr. John Cronan, Jr., and purified as described previously (Nenortas & Beckett, 1996). ^{15}N labeling of BCCP87 was achieved by expression in M9 minimal medium containing 0.1% (w/v) ^{15}N-ammonium chloride and 0.1 mg/mL ampicillin, and supplemented with 0.05% (w/v) thiamin hydrochloride, 0.01% (w/v) each biotin, choline chloride, folic acid, niacinamide, D-pantothenate, and pyridoxal, 0.001% (w/v) riboflavin, 1% (w/v) glucose, 0.002 M magnesium sulfate, 0.0001 M calcium chloride, and 1×10^{-5} M each zinc sulfate, cupric sulfate, ferric chloride, and manganese sulfate. Cells were grown in three stages at 37 °C. A 5 mL starter culture that was incubated for 8 h was used to inoculate a 250 mL culture. After an 8-h incubation, this second culture was equally divided into four portions and added to four 2-L volumes of medium. The final cultures were grown to an optical density at 600 nm of 1.0. Expression was induced by addition of isopropyl β-D-thiogalactoside to 0.5 mM and allowed to proceed for 4 h prior to harvesting the cells. Protein purification was carried out as previously described (Nenortas & Beckett, 1996). The molecular mass of purified apoBCCP87 determined by MALDI-TOFMS agreed with the sequence-calculated molecular mass of the apo form. The activity of apoBCCP87 in the BirA-catalyzed transfer of biotin was measured by a stoichiometric fluorescence titration (Nenortas & Beckett, 1996). A stoichiometry of 1:1 for BCCP87 with the BirA−bio−5′-AMP complex indicated that the purified apoBCCP87 was fully active in the biotin transfer reaction.

Nuclear Magnetic Resonance Spectroscopy. Samples (1.0−2.0 mM) for NMR were prepared in either 95% H_2O/5% D_2O or D_2O, containing 100 mM KCl, 2.5 mM $MgCl_2$, and 10 mM phosphate buffer (pH 7.5 and 6.2). NMR data were collected with General Electric Omega PSG (599.71 MHz, ^1H) with the sample maintained at 25 °C. All experiments were collected with sample at pH 7.5, except that 2D NOESY experiments were collected at both pH 7.5 and 6.2, in an effort to identify fast-exchanging amide protons. Two-dimensional NOESY data were collected with a 150 ms mixing time without presaturation. The 2D homonuclear Hartmann−Hahn (HOHAHA) spectrum was collected using a 76 ms MLEV-17 spin−lock duration. In both experiments, water suppression for samples in water was achieved using WATERGATE read pulses prior to acquisition (Piotto et al., 1992). DQF-COSY spectra were collected with continuous wave solvent presaturation followed by a Scuba pulse train of 40 ms. Two-dimensional ROESY data (Bothner-by et al., 1984) were obtained with a 65 ms spin−lock field of 6 kHz. All of these 2D experiments were also collected with samples in D_2O without water

suppression. For some experiments the initial sampling delay was set to half the t_1 dwell period to eliminate baseline distortions in the *F*1 dimension (Marion & Bax, 1989; Marion et al., 1989a). In many cases, alternate-block acquisition mode was utilized to minimize t_1 noise.

Two-dimensional $^1H-^{15}N$ HSQC and 3D ^{15}N-edited NOESY-HSQC and ^{15}N-edited TOCSY data were acquired with the uniformly ^{15}N-labeled apoBCCP87 sample (95% H_2O/5% D_2O), using water flip-back (Grzesiek & Bax, 1993) and field gradient pulses (Piotto et al., 1992) to suppress the water signal without saturation. The initial ^{15}N evolution period (*F*2) in 2D HSQC and 3D NOESY-HSQC were set to half the dwell time in order to remove baseline distortions (Bax et al., 1991; Zhu et al., 1993). WALTZ-16 (Shaka et al., 1983) modulation was used to decouple ^{15}N during acquisition. A mixing time of 150 ms was used for the 3D ^{15}N-edited NOESY-HSQC. Three-dimensional ^{15}N-edited TOCSY data were obtained with a 50 ms clean-MLEV-17 spin−lock duration (Greisinger et al., 1988) and sensitivity-improved gradient coherence selection (Zhang et al., 1994). For all measurements ^1H carrier was set to the water resonance (4.773 ppm at 25 °C) with 9090 Hz spectral width and 112 ms acquisition time. The ^{15}N carrier was set to 117.8 ppm with 1215 Hz spectral width. Natural abundance $^1H-^{13}C$ HMQC spectra were obtained using samples in D_2O solutions with no water presaturation. ^1H carrier was set to the water resonance.

Two-dimensional proton-detected heteronuclear NMR spectroscopy was used to measure longitudinal relaxation rate constants (R_1), transverse relaxation rate constants (R_2), and $\{^1H\}-^{15}N$ steady-state heteronuclear Overhauser effects (NOE) for the backbone ^{15}N spins of uniformly ^{15}N-labeled apoBCCP87. Relaxation measurements were performed using inversion recovery (Vold et al., 1968), Carr−Purcell−Meiboom−Gill (CPMG) (Carr & Purcell, 1954; Meiboom & Gill, 1958) and steady-state NOE (Noggle & Shirmer, 1971) pulse sequences described previously (Barbato et al., 1992; Farrow et al.; 1994, Kay et al.,1992; Peng & Wagner, 1992). Dipolar relaxation and chemical-shift anisotropy cross-correlation were removed by proton 180° pulses applied every 5−10 ms during relaxation delay. The t_1 evolution is designed as a semiconstant time period to optimize the acquired signal in the t_1 dimension. Decoupling during acquisition was performed using WALTZ16 (Shaka et al., 1983). T_1 and T_2 data were collected with 1 and 1.5 s predelay, respectively. T_1 data were collected at 30, 120, 250, 380, 510, 630, 760, and 1020 ms. T_2 data were collected at 8, 40, 88, 136, 184, 248, 312, and 376 ms. The $\{^1H\}-^{15}N$ steady-state NOE values were obtained by recording spectra with and without the use of proton saturation before the start of the experiment. Data were collected with the water flip-back pulses (Grzesiek & Bax, 1993) and ^{15}N decoupling during acquisitions with 3 s proton saturation and 3 s predelay. All experiments were collected utilizing WATERGATE read pulses to achieve water saturation (Piotto et al., 1992). For all measurements ^1H carrier was set to the water resonance with 9090 Hz spectral width and 112 ms acquisition time. The ^{15}N carrier was set to 117.8 ppm with 1215 Hz spectral width, and 256 complex points were collected starting at half the dwell time with States time-proportional phase incrementation (TPPI) for quadrature detection (Bax et al., 1991; Marion et al., 1989c).

NMR spectra were processed with Silicon Graphics computers using the FELIX software package (versions 95.0; Biosym/Molecular Simulations, San Diego, CA). The 2D NOESY, TOCSY, and COSY spectra were processed using 70°-shifted squared sine bell filtering in t_2 and 60°-shifted squared sine bell in t_1. The 2D $^1H-^{15}N$ HSQC spectrum was processed using 90°-shifted squared sine bell in both t_1 and t_2. Three-dimensional ^{15}N -edited NOESY-HSQC and ^{15}N-edited TOCSY were processed using 60°-shifted squared sine bell on initial 1024 real points in t_3, which became 512 real points after data reduction. For t_1 and t_2, the 3D ^{15}N-edited NOESY-HSQC data were doubled by mirror-image linear prediction in t_2. Data were apodized in t_1 and t_2 by 60°- and 70°-shifted squared sine bell, respectively, and zero-filled to 512 and 128 real data points, respectively. Three-dimensional ^{15}N-edited TOCSY data were linear-predicted in t_1 and t_2 to 64 and 192, respectively, and apodized by 75°-shifted squared sine bell, with zero-filling to 128 and 512, respectively. T_1, T_2, and NOE spectra were processed with 70°-shifted squared sine bell in both dimensions and zero-filled to 512 in the ^{15}N dimension.

All data analysis was done with NMRVIEW software (Johnson & Blevins, 1994). For T_1 and T_2 dynamics measurements, cross-peak intensities were measured from peak heights and fit to an exponential decay function by nonlinear least-squares analysis using the Levenburg−Marquardt method (Press et al., 1992). NOE values were determined as the ratios of the peak intensities measured from spectra acquired with and without saturation during the recycle delay.

Structure calculations were carried out using the DIANA software package (Güntert & Wüthrich, 1991; Güntert et al., 1991). Distance restraints of 1.8−2.7 Å, 1.8−3.3 Å, and 1.8−5.0 Å were employed for cross-peaks of strong, medium, and weak intensity, respectively, observed in the NOE spectra. An additional 0.5 Å was added for NOEs involving methyl protons (Clore et al., 1987), 0.8 Å was added for NOEs involving methylene protons, and 1.5 Å was added for NOEs involving degenerated valine methyls.

Structures were generated from random initial coordinates using DIANA calculations and refinement of models was carried out using the strategy of redundant dihedral angle constraints (REDAC) (Güntert & Wüthrich, 1991; Güntert et al., 1991) with different minimization parameters. NOE-derived and primary distance restraints were given equal weighting during the final stage of structure calculations. Separate calculations with and without hydrogen-bonding restraints were performed.

RESULTS

NMR Spectra and Assignments. NMR studies were carried out with nonlabeled and ^{15}N isotopically labeled recombinant apoBCCP87 protein samples. This C-terminal domain fragment has been shown to be as active as the intact apoBCCP protein in the BirA-catalyzed biotin ligation reaction (Nenortas & Beckett, 1996). Signal assignments were made by analysis of 2D homonuclear correlated data (Wüthrich, 1986), combined with ^{15}N-edited 2D and 3D heteronuclear data (Marion et al., 1989b). Figure 2 shows the $^1H-^{15}N$ heteronuclear single quantum coherence (HSQC) spectrum of ^{15}N-isotopically labeled apoBCCP87 acquired in buffer conditions identical to those used for the unlabeled

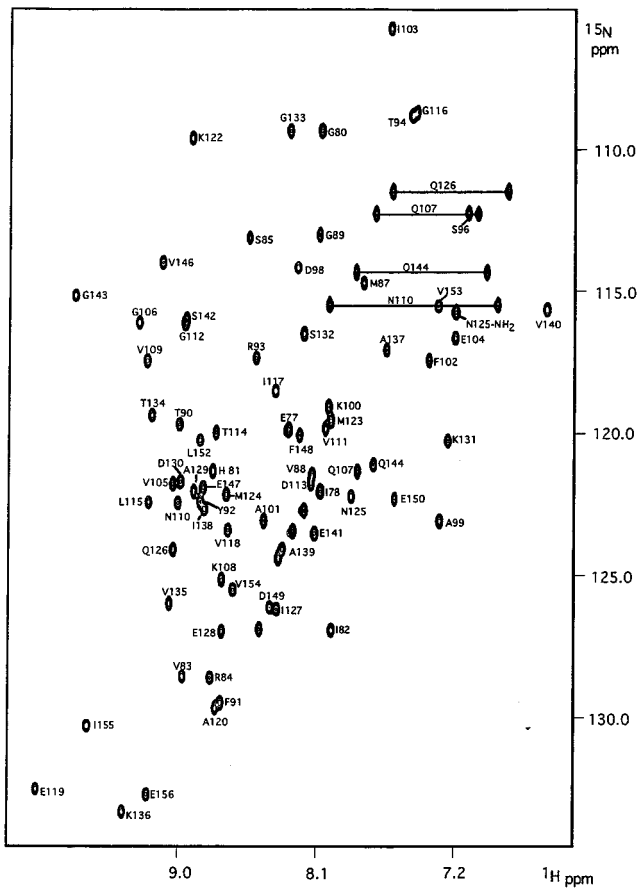

FIGURE 2: Portion of the 2D $^1H-^{15}N$ HSQC spectra of ^{15}N-apoBCCP87 (pH 7.5, T = 25.0 °C, 95% H_2O/5% D_2O). The spectrum shows $^1H-^{15}N$ correlations for 74 of the non-proline residues. Solid lines indicate side-chain NH_2 groups of Asn and Gln residues. N-Terminal residues Met70−Ala76 and Ser79 could not be unambiguously assigned due to lack of NOE signals. In addition, Met121 was not identified in data collected at pH 7.5 due to solvent exchange.

sample. Amide signal degeneracies in 2D NOESY and TOCSY were largely eliminated in the $^1H-^{15}N$ correlated NMR data (Griesinger et al., 1988; Kay et al., 1989a). With the ^{15}N-edited NOESY and ^{15}N-edited HOHAHA, sequential NH−NH, NH−H^α, or NH−H^δ (for proline residues) connectivities were observed for 79 of the total 87 residues, enabling proton NMR signal assignments to be made via sequential assignment strategies (Wüthrich, 1986). The N-terminal residues Met70−Ala76 and Ser79 could not be unambiguously assigned due to lack of NOE signals, indicating that this segment is flexible in solution. In addition, no NMR signal was detected for the backbone amide proton of Met121 at pH 7.5, mainly due to exchange with solvent. It was identified in data collected in buffer at pH 6.2, in which amide proton exchange is slower.

Many of the α-protons close to the water signal could not be identified from data collected with the sample in water and were recovered and assigned from 2D NOESY and Clean-HOHAHA spectra collected with the sample in D_2O. Most of the proline α and δ protons were also assigned. In several cases, side-chain protons of residues with longer side chains could not be assigned unambiguously due to signal degeneracies and overlap in the upfield region of the double-quantum filtered correlated (DQF-COSY) data (Rance et al., 1983). For many residues, nearly equal-intensity NOE cross-peaks were observed for dipolar interaction involving prochiral protons. Thus only 26% of the prochiral protons in the Glu77−Glu156 stretch were specifically assigned. ^1H and ^{15}N chemical shift assignments are available in the supporting information.

Secondary Structure Determination and Proton Chemical Shift Analysis. Elements of regular secondary structure were identified on the basis of cross-peak patterns and intensities observed in the 2D homonuclear NOESY and the 3D ^{15}N-edited NOESY spectra. NOE intensities were qualitatively grouped into strong, medium, and weak categories. The NOE cross-peak patterns and corresponding secondary structural elements, are summarized in Figure 3. With the exception of Leu115−Cys116, Lys136−Ala137, and Leu152−Val153 proton pairs, strong sequential H^α−NH ($H^\alpha-H^\delta$ for proline residues) NOE connectivities observed for residues Gly80−Ser85, Val88−Tyr92, Gln107−Asn110, Asp113−Ala120, Met123−Ala129, Gly133−Ile138, Gln144−Glu147, and Glu150−Glu156 indicate that these segments exist in an extended conformation. This description of secondary structure is in good agreement with that of the crystal structure (strands $\beta1-\beta8$) (Athappilly & Hendrickson, 1995). Strong sequential NH−NH NOE connectivities for Leu115−Cys116, Lys136−Ala137, and Leu152−Val153 proton pairs suggest that these residues form bulges within three of the β-strands. Strong interstrand $H^\alpha-H^\alpha$ NOEs characteristic of antiparallel β-sheet structure further indicate that the eight β strands form two four-stranded β-sheets, with $\beta1$, $\beta3$, $\beta6$, and $\beta8$ forming one sheet and $\beta5$, $\beta4$, $\beta2$, and $\beta7$ forming the other. These two four-stranded antiparallel β-sheet structures are schematically shown in Figure 4.

NOE cross-peaks characteristic of type II turns (Wüthrich, 1986) were observed for residues Val105−Gln107, Val111−Asp113, Glu147−Glu150, and Ser142−Gln144. Thus, consistent with the X-ray structure (Athappilly & Hendrickson, 1995), $\beta3$ and $\beta7$ are each bracketed by two type II turns. Lys122, the biotin acceptor, is located in a β turn between $\beta4$ and $\beta5$ (Figure 5). Medium to strong intensity Lys22-NH−Met123-NH, weak intensity Met121-NH−Lys122-NH (due to solvent exchange of Met121-NH), and medium sequential Lys122-Hα−Met123-NH NOE cross-peaks are indicative of a type I′ turn. Finally, residues Arg93−Phe102 form a protrusion, in which residues Ser96−Ala99 form a β turn. However, due to solvent exposure, the weak amide signals associated with the residues composing this turn precluded unambiguous identification of the β turn type.

It has previously been shown that NMR chemical shifts for backbone H^α atoms correlate well with secondary structure (Spera et al., 1991; Wishart et al., 1991, 1992). Therefore, chemical shift values of the H^α resonances of apoBCCP87 were compared with the values consistent with random coil structure. The resulting secondary shifts agree with the secondary structure derived from the NOE data (Figure 3). Specifically, residues His81−Arg84, Val88−Tyr92, Lys108−Asn110, Ile117−Ala120, Ser132−Ile138, Gln144−Glu148, and Leu152−Glu156 exhibit positive secondary shifts consistent with an extended secondary structure. Thus, although several residues exhibit shift differences, the H^α secondary chemical shifts for β-sheets are generally consistent with an extended conformation.

Structure Determination. A total of 614 interproton distance restraints derived from 2D and 3D NOE data were employed for structure calculations, including 13 intraresidue,

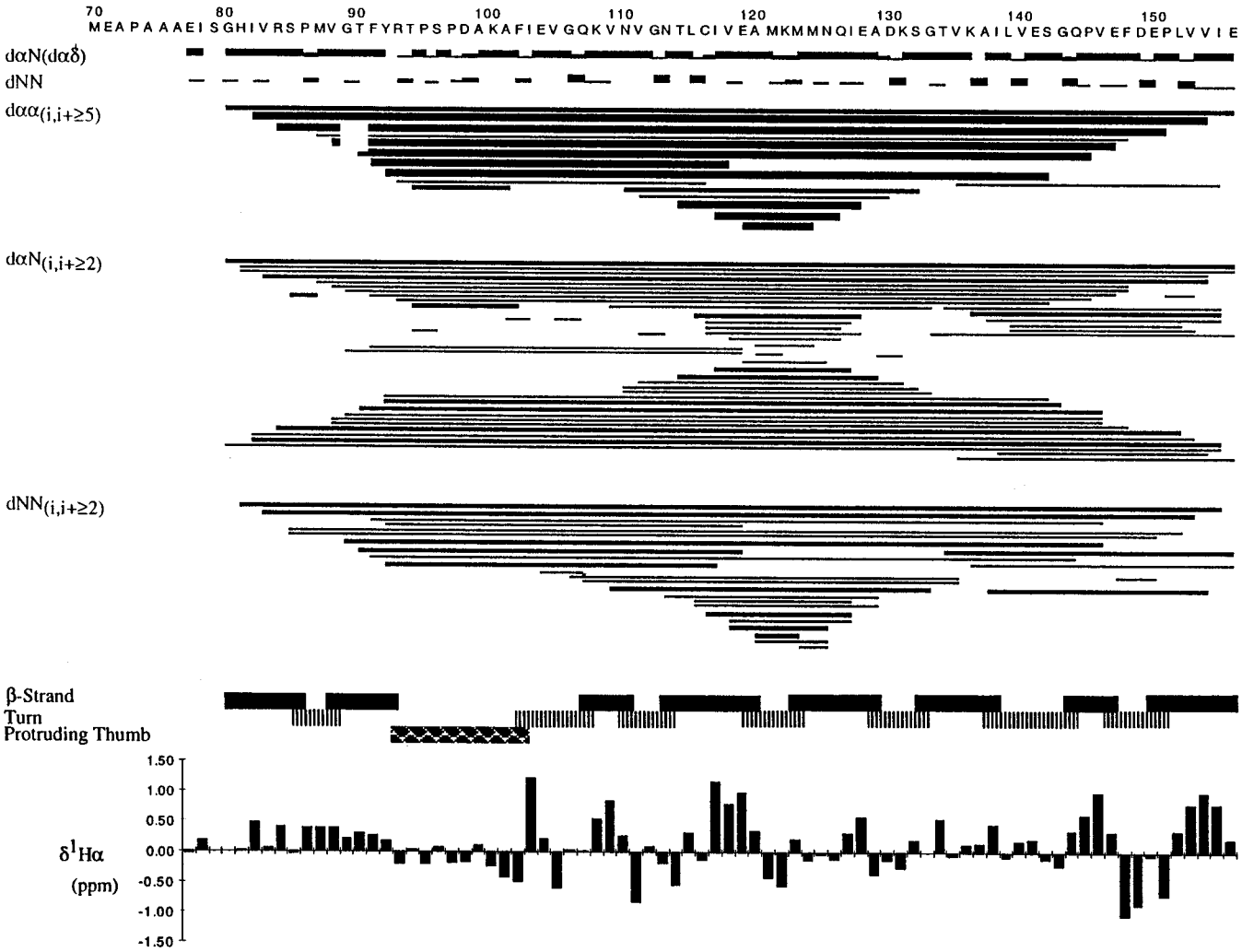

FIGURE 3: Summary of $H^{\alpha}-NH$, $NH-NH$, and $H^{\alpha}-H^{\alpha}$ NOE connectivities identified from 2D NOESY and 3D $^{1}H-^{15}N$ NOESY-HSQC spectra of apoBCCP87. The thickness of the horizontal bars denotes the relative intensities of the NOE cross-peaks. The secondary structural elements are also shown. The α-proton secondary chemical shifts are shown at the bottom of the figure. Groupings of downfield-shifted protons (>0) correspond to β-strand type structure.

194 sequential, 66 medium-range (2−5 residues), and 256 long-range interproton distance restraints and 84 NH−O and N−O hydrogen-bond restraints (Table 1). Hydrogen-bond restraints were determined from analysis of the NOE-derived secondary structure. Protons that exhibit NOE cross-peaks to a specific prochiral proton often give a signal to the neighboring prochiral proton, and in the present studies, restraints were not included for the weaker of two such cross-peaks. Restraints for moderate or weak intraresidue cross-peaks, which do not serve a useful function in the structure calculations, were also not included. No intraresidue restraints were imposed for side-chain protons with undefined stereochemistry. Thus, many cross-peaks observed in the NOE spectra were not used as distance restraints. On average, a total of 15.4 distance restraints/assigned residue were used for structure calculations. The total number of NOE-derived interproton distance restraints as a function of residue number is shown in Figure 6.

All structure calculations were performed using the variable target function program DIANA (Güntert & Wüthrich, 1991; Güntert et al., 1991). A family of 58 refined conformers were generated using the strategy of redundant dihedral angle constraints (REDAC) (Güntert & Wüthrich, 1991; Güntert et al., 1991). Statistical information for structure calculation is reported in Table 1. Of these, individual distance violations were 0.11 Å or less and penalty values (= squared sum of all distance violations) were 0.008−0.039 $Å^2$. Of these, nine structures were generated without hydrogen-bond restraints. Models generated with and without hydrogen-bond restraints exhibit the same three-dimensional structures. Superposition of residues 80−156 of all 58 models afforded an average pairwise rms deviation of 0.60 (± 0.14) Å. Since the biocytin turn and the protruding thumb are less well defined, superposition of the backbone heavy atoms (C, C^{α}, and N) of restrained residues Gly80−Arg94, Lys100−Ala120, and Met123−Glu156 of all 58 structures afforded an average pairwise rms deviation of 0.52 (± 0.11) Å (Table 1, Figure 7). Superposition of the models generated with hydrogen-bond restraints for the same stretch of residues afforded better convergence, with an average pairwise rms deviation of 0.48 (± 0.09) Å.

Three-Dimensional Structure and Dynamical Properties of ApoBCCP87. ApoBCCP87 consists of two four-stranded antiparallel β-sheets that are packed together via a hydrophobic core, forming two symmetrical halves of the molecule (Figure 8, top). A hairpinlike protrusion connects the two halves. The entire molecule can be described as an antiparallel β-barrel, with strands β1, β8, β6, and β3 forming one β-sheet and strands β5, β4, β2, and β7 forming the other. The curvature of β2 makes it possible for it to pair with β4

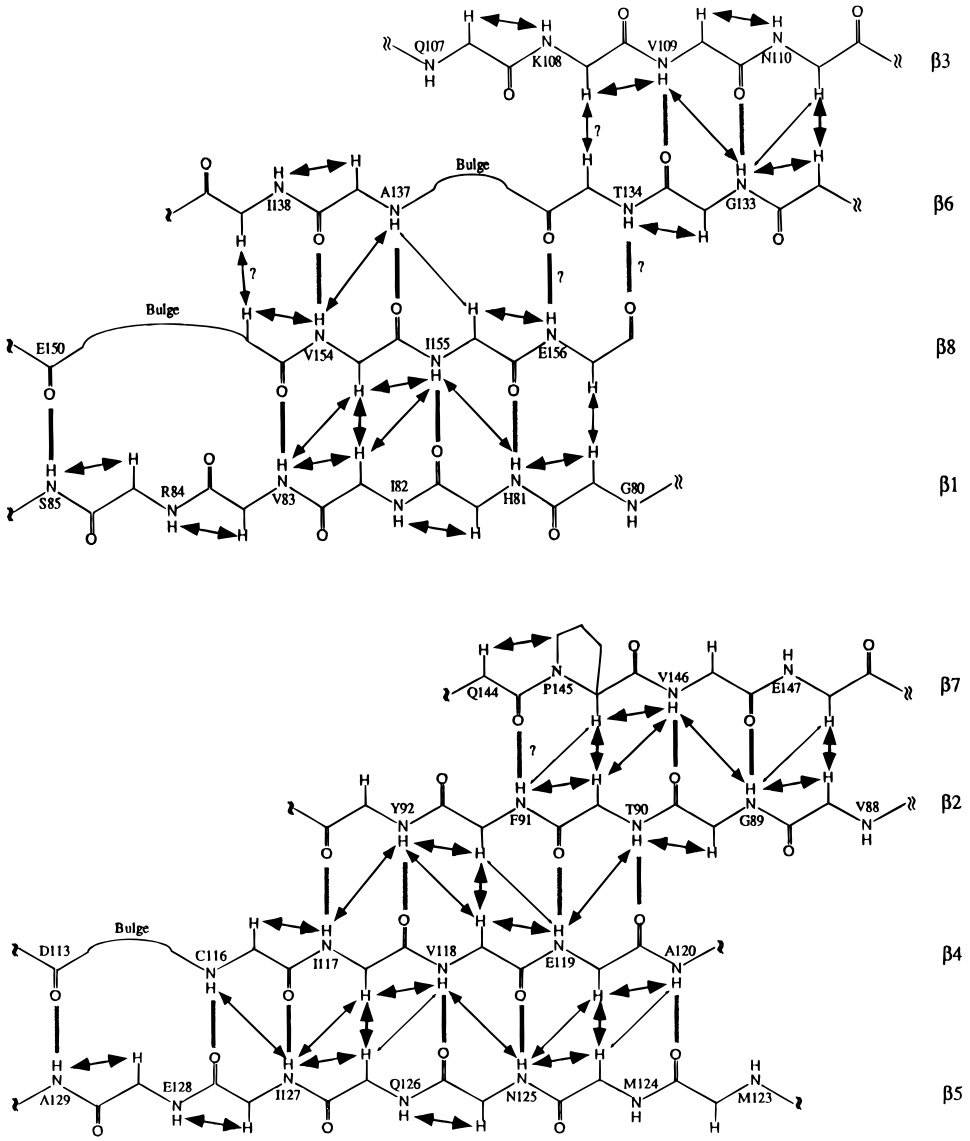

FIGURE 4: Schematic representation of the characteristic NOE connectivities (arrows) that define the two four-stranded antiparallel β-sheets in apoBCCP87. The thickness of the arrows is proportional to the intensity of the cross-peaks. Hydrogen bonds deduced from the NOE data and modeling studies are denoted as lines. Question marks indicate hydrogen bonds for which insufficient evidence is available due to signal degeneracy or overlap. These were not included in structural calculation.

at one end, which further pairs with β5 to form the flat region of the β-sheet. The β2 strand pairs with β7 at the other end, which is almost perpendicular to the flat segment of the sheet and thus forms a cap of the β-barrel. The counterpart of β2, β6, pairs with β8 at one end, which further pairs with β1. The β6 strand pairs with β3 at the other end and forms the second cap of the β-barrel.

The single cysteine residue, Cys116, is buried in the hydrophobic core formed by residues Ser85, Pro86, Phe91, Ile103, Val109, Leu115, Ile117, Val118, Ile127, Ala129, Val135, Val146, Leu152, Val153, and Ile155, as shown in Figure 8 (bottom). Most of these hydrophobic residues are very well defined and presumably play an important role in stabilizing the β-barrel structure.

The NMR relaxation parameters, longitudinal relaxation time constants (T_1), transverse relaxation time constants (T_2) and steady-state $\{^1H\}-^{15}N$ nuclear Overhauser effects (NOE) were obtained by analysis of two-dimensional proton-detected heteronuclear NMR spectroscopy, using ^{15}N isotopically labeled recombinant apoBCCP87 protein samples at pH 7.5. Quantitation of peak intensities from measurements of peak heights were made for 73 ^{15}NH backbone resonances (87 residues minus eight unassigned residues, Met121, and five proline residues). Uncertainties in the peak heights were estimated on the basis of the root-mean-square baseline noise in the spectra (Palmer et al., 1991). The relaxation data are plotted in Figure 9.

The procedure outlined by Mandel et al. (1995) was followed in analysis of the T_1, T_2, and NOE data. The "model-free" approach of Lipari and Szabo (1982) was used to analyze the relaxation data. The ^{15}N T_1/T_2 ratio is, to a good approximation, independent of rapid internal motions, because these motions increase the T_1 and T_2 values uniformly (Kay et al., 1989b). This enables calculation of the overall rotational correlation time τ_m from the T_1/T_2 ratio. However, care must be taken when using this method. First, residues with NOE values less than 0.6 should be excluded from such analysis, because for such residues the assumption that rapid internal motions do not affect the T_1/T_2 ratio is invalid. Consequently, the N-terminal residues E77, I78, and G80 were not included in the analysis of the relaxation data. Omitting the data for these three residues, the mean values

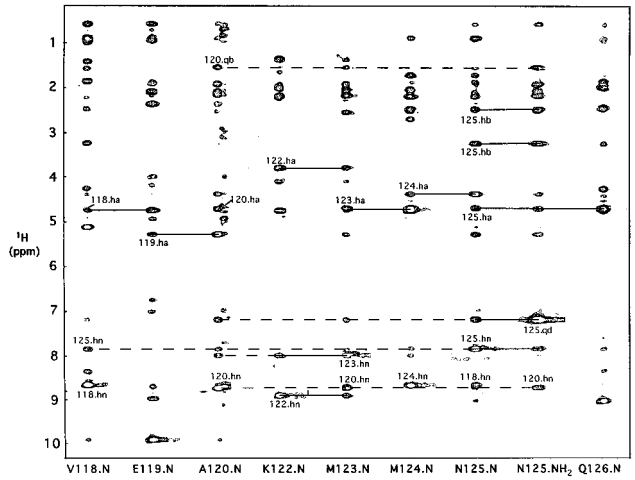

FIGURE 5: Strips from the 3D ^{1}H−^{15}N NOESY-HSQC spectrum of ^{15}N-apoBCCP87 (pH 7.5, $T = 25.0$ °C, $t_m = 150$ ms, 95% H_2O/5% D_2O) taken at the ^{15}N chemical shifts of residues Val118−Gln126 (except for Met121) and Asn125-NH_2, corresponding to the biocytin turn and adjacent residues from β4 and β5. Solid lines indicate sequential H^α−NH and NH−NH connectivities. Dotted lines indicate long-range NOE connectivities characteristic of antiparallel β-sheet. The NOEs between the $H^{\delta 2}$ protons of Asn125 with the backbone amide proton and the methyl group of Ala120, which suggest a superhelical twist of the β-sheet structure (see text), are also shown as dotted lines.

for T_1, T_2, and NOE were 0.53 (± 0.06) s, 0.14 (± 0.01) s, and 0.74 (± 0.05), respectively. Second, slow conformational exchange shortens the value of T_2 but not of T_1. Therefore, a smaller than average value of T_2 in the absence of a concomitant increase in T_1 is indicative of conformational exchange (Tjandra et al., 1996). According to this criterion, residues for which the T_2 value was affected by conformational exchange were excluded from the calculation, using the following relationship (Tjandra et al., 1995, 1996):

$$(\langle T_2\rangle - T_{2n})/\langle T_2\rangle - (\langle T_1\rangle - T_{1n})/\langle T_1\rangle > 1.5\mathrm{SD}$$

where T_{2n} and T_{1n} are the measured values for residue n, $\langle T_2\rangle$ and $\langle T_1\rangle$ are the mean values given above, and SD is the standard deviation of $(\langle T_2\rangle - T_{2n})/\langle T_2\rangle - (\langle T_1\rangle - T_{1n})/\langle T_1\rangle$. On the basis of this equation, residues Asp98, Asp113, and Met124 were excluded. For the remaining residues, the average value of the T_1/T_2 ratio, 3.6 (± 0.3), was used to estimate the overall rotational correlation time $\tau_m = 5.1$ (± 0.3) ns (Palmer et al., 1991).

Selection of model-free parameters for each nuclear spin was carried out using the statistical strategy outlined in Mandel et al. (1995). Of the 73 backbone ^{15}N nuclear spins, relaxation data for a total of 38, 8, 10, 7, and 10 backbone ^{15}N atoms were fit by models 1−5, respectively, where model 1 fits only the generalized order parameter (S^2), model 2 fits S^2 and the effective internal correlation time (τ_e), model 3 fits S^2 and the chemical exchange term (R_{ex}), model 4 fits S^2, τ_e, and R_{ex} terms, and model 5 fits order parameters of internal motions on both fast and slow time scales (S_f^2 and S_s^2, respectively) and also τ_e. After final optimization with the selected model for each nuclear spin, the global τ_m was 5.05 (± 0.02) ns. The sum-squared error (SSE) values for 58 nuclear spins were less than the $\alpha = 0.05$ critical value; five nuclear spins had SSE values slightly greater than the critical values; 10 had SSE values in the range 8−20. Excluding these latter 10 nuclear spins, the average values of SSE were 2.14, 1.37, and 0.00 for models with two (model 1), one (models 2 and 3), and zero (models 4 and 5) degrees of freedom, respectively.

Table 1: Distance Restraints and Structural Statistics[a]

Distance Restraints	
intraresidue	13
sequential	194
medium-range ($\|i-j\| = 2-5$ residues)	66
long-range ($\|i-j\| > 5$ residues)	256
hydrogen bonds	84
total NMR-derived restraints	614
mean restraints/residue[b]	15.4
Distance Violations[c,d]	
mean total penalty (Å^2)	0.022 ± 0.08
maximum total penalty (Å)	0.039
minimum total penalty (Å)	0.008
maximum individual violation (Å)	<0.11

	pairwise RMS deviations[a] (Å)		
	all	H-bonds	no H-bonds
backbone heavy atoms (C, C^α, and N)			
residues 80−94, 100−120, and 123−156[f]	0.52 ± 0.11	0.48 ± 0.09	0.63 ± 0.10
residues 80−156[g]	0.60 ± 0.14	0.56 ± 0.11	0.77 ± 0.14
all atoms			
residues 80−94, 100−120, and 123−156[f]	1.62 ± 0.12	1.60 ± 0.11	1.63 ± 0.12
residues 80−156[g]	1.72 ± 0.14	1.69 ± 0.14	1.80 ± 0.16

[a] Penalty (equal to the squared sum of the distance violations) and RMSD values are in units of squared angstroms and angstroms, respectively; distance violations are in units of angstroms. Values are reported as a mean ± standard deviation. [b] Calculated for 79 restrained residues. Each interresidue restraint was counted twice to determine the mean number of restraints per residue. [c] Results for 58 structures generated by the program DIANA (distance geometry algorithm for NMR applications), including 49 generated with H-bond restraints and nine generated without H-bond restraints. [d] Values are reported as a mean ± standard deviation. Penalty = sum of the square of all distance violations. [e] Pairwise rms deviations calculated for the given range of residues for structures generated with H-bond restraints, without H-bond restraints, and for the entire family of 58 models. [f] Residues comprising all the regular secondary structure, excluding poorly defined residues in the protruding thumb (residue 95−99) and the biocytin turn (residue 121−122). [g] The entire folded apoBCCP87.

Optimized values of the model-free parameters are presented in the supporting information. The generalized order parameters S^2, the internal correlation time τ_e, and the chemical exchange terms R_{ex} for the backbone ^{15}N nuclear spins are plotted as a function of the residue number in Figure 9. The average value of the order parameter for all 73 measured residues is 0.8 (± 0.1) and they range from 0.75 to 0.89 for each of the eight β stands, with β1 and β5 characterized by the lowest values of 0.80 (± 0.05) and 0.75 (±0.07), respectively. The relatively low order parameter for β1 was expected because of its location near the N-terminus, whereas the reduced S^2 value for β5 is of interest, as discussed later. The increased average order parameter of 0.89 (± 0.07) for β8 is mainly due to the unusually high value for residue Glu150 ($S^2 = 1.000 \pm 0.007$).

Low order parameters (0.26−0.39) were observed for N-terminal residues Ile77, Glu78, and Gly80. This result is consistent with the NOE, chemical shift, and modeling data, which indicate that the N-terminal residues are disordered. Two additional regions of the protein exhibit lower-than-average order parameters, including the biotin-binding turn (and the following strand β5) and the protruding thumb (residues Thr94−Ala101) (Figure 9). The order parameter

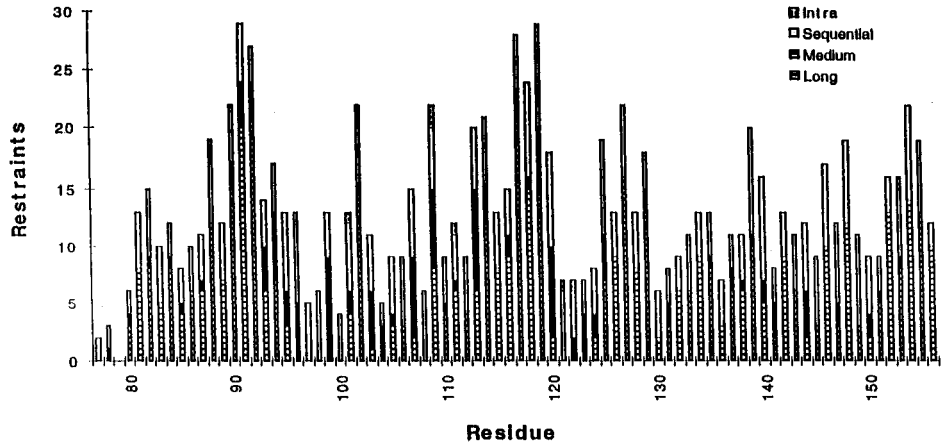

FIGURE 6: Plot showing the number of intraresidue (bar enclosing dashed line), sequential (i to $i + 1$) (open bar), medium-range [i to $i +$ (2−5)] (solid bar) and long-range (i to $i + >5$) (horizontally striped bar) NOE-derived interproton distance restraints per residue employed for structural calculations of apoBCCP87.

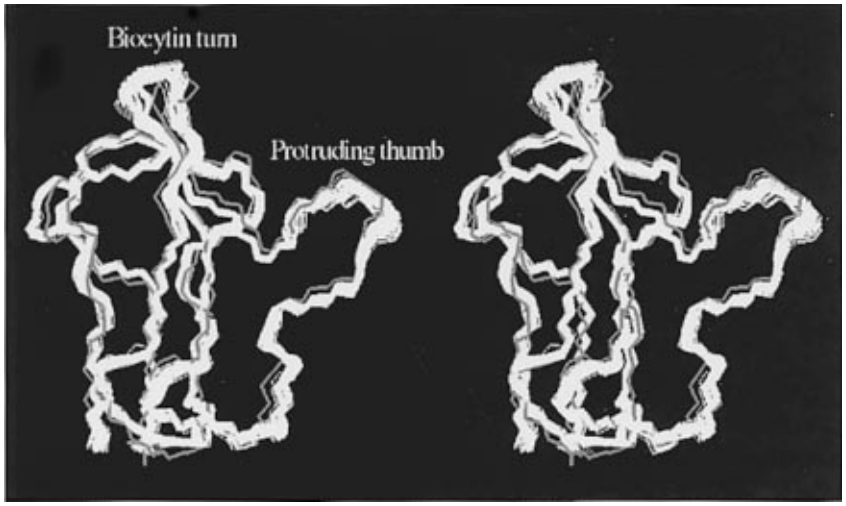

FIGURE 7: Stereoviews of the best-fit superpositions of the backbone heavy atoms (C, C^{α}, and N, residues Gly80−Thr94, Lys100−Ala120, and Met123−Glu156) of the 49 refined apoBCCP87 models (yellow) generated with hydrogen bond restraints, and the model derived from the X-ray crystallographic structure of holoBCCPsc (blue), illustrating the conformational differences between the NMR and crystal models. Figures were generated with the MOLMOL software package.

for Lys122 is 0.81 (± 0.02) and values for residues Met123−Ala129 of β5 range from 0.65 to 0.80. In the protruding thumb, residues Ser96−Ala99, which form a β turn, exhibit significantly lower order parameters (0.52−0.79) with an average S^2 of 0.7 (± 0.1). The reduced order parameters for these regions indicate enhanced mobility on the picosecond to nanosecond time scale. The increased mobilities are accompanied by conformational exchange or amide proton exchange terms for residues Met123 and Met124 in strand β5 and Ser96, Asp98, and Ala101 in the protruding thumb. For example, residue Met124 has one of the lowest order parameters ($S^2 = 0.65 \pm 0.02$) and a relatively high chemical exchange term (1.4 ± 0.3). With the exception of the N-terminal residues, residue Asp98 has the lowest order parameter ($S^2 = 0.53 \pm 0.04$) and highest chemical exchange term (1.7 ± 0.4). These results imply increased internal motion as well as extensive conformational dynamics on the chemical exchange time scale.

DISCUSSION

The structure of the apoBCCP87 presented in this work and that of the holoBCCPSC determined by Athappilly and Hendrickson (1995) are very similar. The X-ray crystal structure was determined on a proteolytic fragment (residues 77−156) obtained from subtilisin digestion of intact BCCP. The NMR structure was determined for a recombinant 87 residue C-terminal fragment of BCCP (residues 70−156). The two proteins thus differ in length by seven residues at the amino terminus. Residues 77−79 at the N-terminus of holoBCCPSC are extended in the crystal structure and do not interact with the main body of the protein. The 10 N-terminal residues of apoBCCP87 are disordered in the NMR structure; thus, differences in the N-terminal residues of the protein should not adversely affect comparison of the apo- and holo-form structures.

Superposition of the backbone heavy atoms (residues 80−156) of the apoBCCP87 NMR structures with the X-ray structure of holoBCCPsc (Athappilly & Hendrickson, 1995) (Figure 7) afforded an average rms deviation of 1.21 Å. The agreement between the apo and holo structures improves significantly when the residues of the β turn containing the biotinylation target, lysine 122, and the "protruding thumb" region are not included in the fitting (rms deviation = 1.07 Å). Detailed comparison of the structures reveals that in apoBCCP87 the β turn containing the biotin moiety assumes an orientation different from that in the crystal structure, with

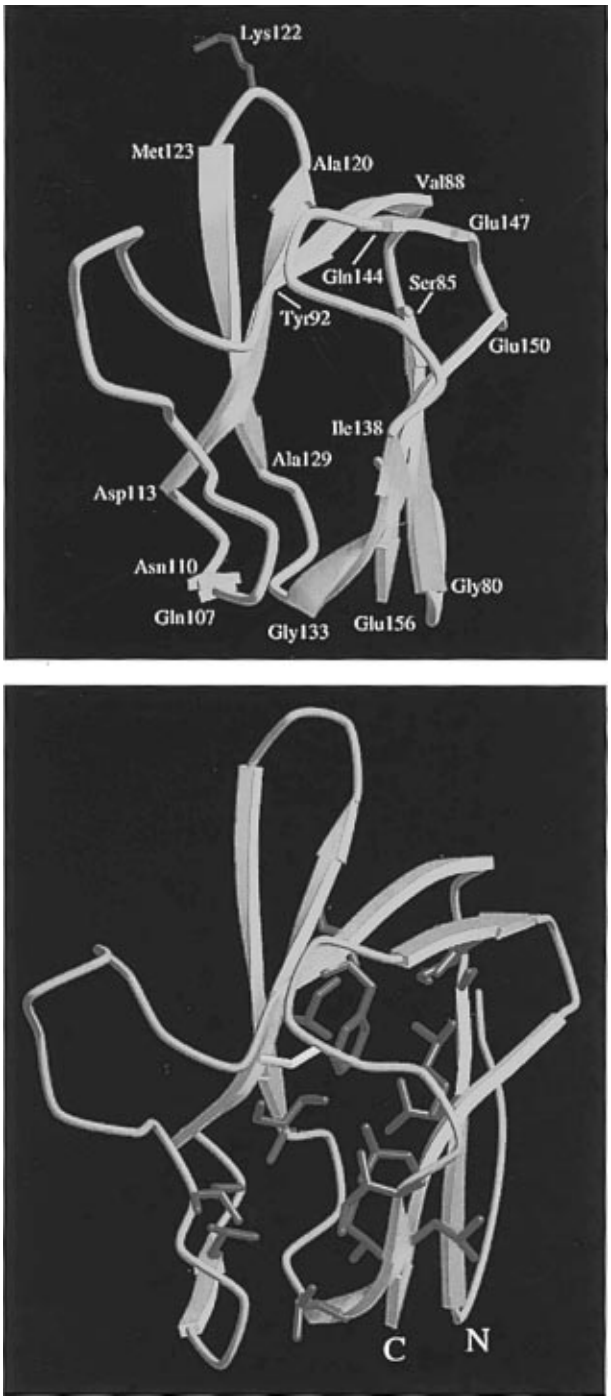

FIGURE 8: Ribbon drawing of the apoBCCP87 structures with the lowest distance restraint violations. Drawings were generated and rendered with (top) MOLSCRIPT (Kraulis, 1991) and (bottom) Raster3-D (Bacon & Anderson, 1988) software packages. (Top) View of the eight β strands showing the symmetrical nature of the structure. Residues defining each β strand are labeled. Shown also is the biotin-binding residue Lys122 in blue. (Bottom) View of the residues comprising the hydrophobic core (green) and the single cysteine residue Cys116 (yellow).

main differences observed at residues Met121 and Lys122. The biocytin residue in BCCPsc is located at a type I′ β turn, which is stabilized by three hydrogen bonds formed between the backbone amide protons of Ala120, Lys122, and Met123 and the carbonyl oxygens of Met123, Glu119Oϵ2, and Ala120, respectively. This pattern is also observed in apoBCCP87, with the exception of the Lys122 and Glu119Oϵ2 pair, which, as indicated by the NOE data, are further apart. In addition, several proton pairs that are well within 5 Å distance in the crystal structure, including Ala120-NH−Met121-NH (3.9 Å) and Ala120-NH−Lys122-NH (3.73 Å), do not show any observable NOE cross-peaks in apoBCCP87 (Figure 5). Furthermore, the superhelical twist at the end of the β4−β5 β hairpin, supported by NOEs between the Hδ2 protons of Asn125 with the backbone amide proton and the methyl group of Ala120 observed in apoBCCP87 (Figure 5), is not observed in the crystal structure. Rather, in the holoprotein the side chain of Asn125 points away from the β sheet, and the type I′ turn forms a plane almost perpendicular to the β sheet. This allows the ureido ring of biocytin to interact with the hairpin protrusion formed by residues Arg93−Phe102. Small differences are also observed between the protruding thumb region of the NMR and X-ray structures, but these differences were too small to be confirmed unambiguously from the NOE data.

To further explore the orientation of the local structure of apoBCCP87 versus holoBCCPsc, we used PROCHECK (Laskowski et al., 1993) to evaluate the backbone torsion angles of residues in the biotin-binding loop. Interestingly, three of the four residues involved in the β turn in the holoBCCPsc X-ray structure, including residues Ala120−Lys122, have relatively unfavorable values of ϕ and Ψ angles compared to the other residues in the structure. In apoBCCP87, however, only Met121 has a less favorable conformation relative to the other residues of the hairpin. The unfavorable conformation of this residue in the apoprotein could reflect the limited number of distance restraints employed in the structure calculation of this residue, due to its rapid intrinsic NH exchange rate. We propose that the conformational differences between the holo- and apoproteins are due to formation of multiple interactions between the ureido ring of the biotin moiety and the residues in the protruding thumb in the holo protein. These multiple interactions appear to confer a strained conformation on the biocytin turn, which does not exist in the apoprotein.

It is also conceivable that the biotinyl group could be disordered in solution and that the interactions with the protruding thumb region observed in the crystal structure are due to crystallization effects. However, comparison of fluorescence emission spectra of the apo and holo forms of the protein indicates that biotinylation results in a 2-fold increase in the quantum yield of the intrinsic protein fluorescence (Wei and Beckett, unpublished results). This increase in the fluorescence intensity is consistent with an average solution conformation of the biotin moiety similar to that observed in the crystal structure of holoBCCP. Bridging of the biotin across the biocytin turn and the protruding thumb apparently results in protection of the single tyrosine residue (Tyr92) from solvent quenching.

The NMR relaxation data obtained for apoBCCP87 reveal that the β turn containing Lys122 and the protruding thumb exhibit rapid internal motions. These segments were shown to have multiple biotin-mediated interactions in the crystal structure of the holoBCCPSC (Athappilly & Hendrickson, 1995). The qualitative agreement of relaxation data of the apo form and crystallographic *B*-factors of the holo form suggests that the inherent mobility of these two regions is not totally lost upon biotinylation of the protein. However, quantitative comparison of the dynamic features of the two forms of the protein awaits solution NMR studies of holoBCCP87.

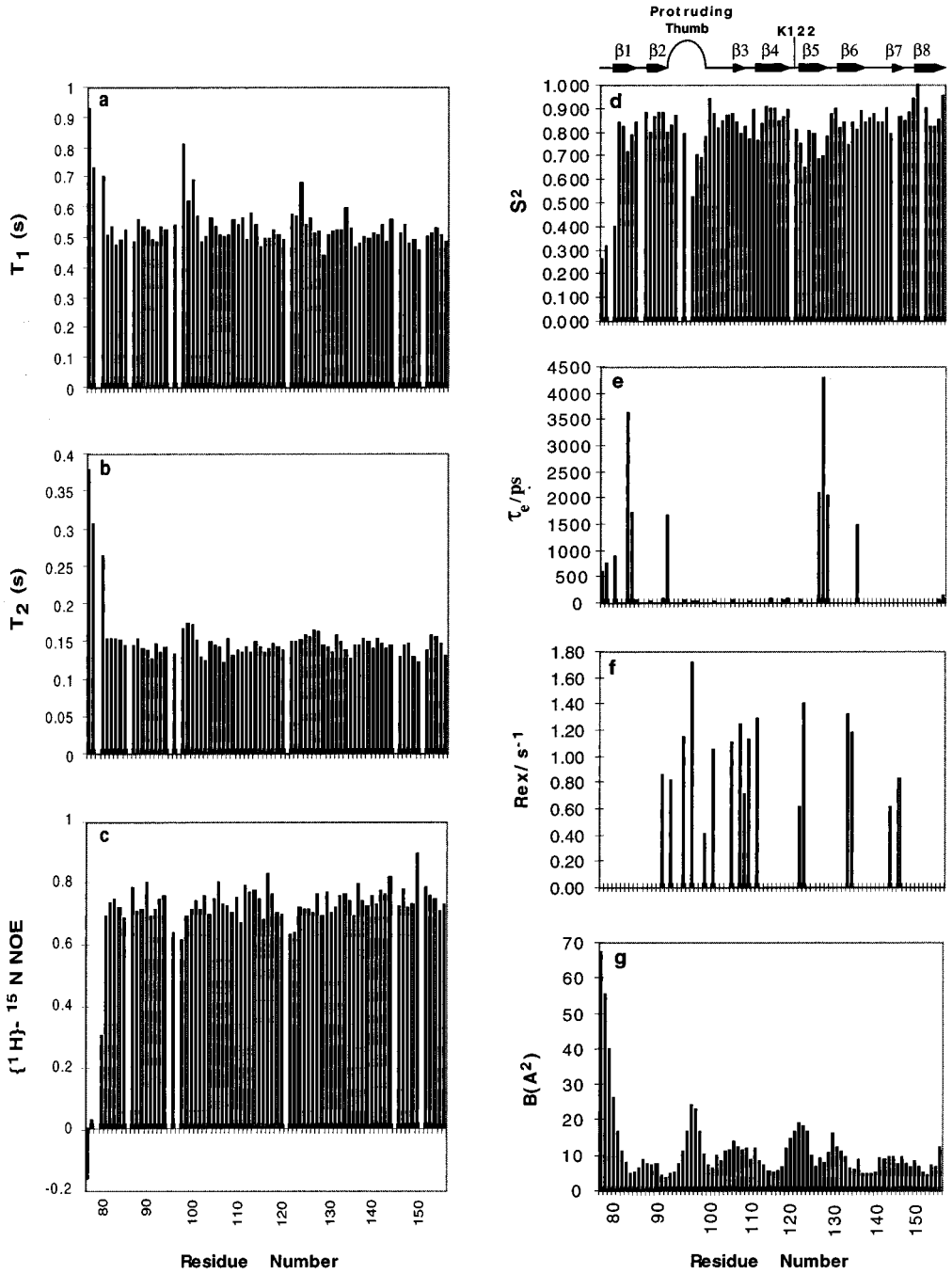

FIGURE 9: Relaxation parameters for apoBCCP87. Shown are (a) the longitudinal relaxation time T_1, (b) the transverse relaxation time T_2, and (c) $\{^1H\}-^{15}N$ NOE values plotted for the 73 residues measured (residues 77−156, excluding Ser79, Met121, and five proline residues), on the left-hand side, and comparison of (d) generalized order parameters S^2, (e) the internal correlation time τ_e, and (f) the chemical exchange term R_{ex}, obtained for backbone ^{15}N spins of apoBCCP87 (residues 77−156, excluding Ser79, Met121, and five proline residues) by model-free analysis, and (g) crystallographic *B*-factors for holoBCCPsc (residues 77−156), on the right-hand side. The diagram above panel d is a schematic representation of the secondary structure.

In its functional cycle the biotin carboxyl carrier protein engages in heterologous protein−protein interactions with three distinct partners. Interaction with the biotin holoenzyme synthetase, BirA, is required for conversion of apoBCCP to the holo form. The biotin carboxylase subunit binds to the holoBCCP in the incorporation of the carboxylate group of bicarbonate into biotin. Finally, the carboxybiotinylated form of BCCP interacts with transcarboxylase in the conversion of acetyl-CoA to malonyl-CoA. Results of biochemical and genetic studies indicate that, in addition to the biotin moiety, amino acid determinants on BCCP are critical for all of these interactions. Li and Cronan (1992) have shown that greater than 76 C-terminal residues of BCCP are required for BirA-catalyzed biotinylation in vivo. Moreover, measurements of biotin carboxylase-mediated carboxylation of holoBCCP87 are significantly faster than those measured for free biotin (Grover Waldrop, personal communication).

The data presented in this study provide evidence for a small, local conformational change upon protein biotinylation. This conformational change may be important for mediating specific interactions relevant to binding of BirA and subsequent biotin transfer. The ureido functionality of biotin appears to be critical for adoption of this second

conformation of BCCP since it forms multiple hydrogen-bonding interactions with the "protruding thumb" region of the protein. Biotin carboxylase-mediated carboxylation of the biotin moiety is expected to disrupt the interaction of the ureido group with the protein and could lead to a third conformation required for optimal interaction of BCCP with transcarboxylase. The prediction of the existence of this third conformation can be tested by determination of the structure of the carboxybiotinylated BCCP87.

Biotin-dependent carboxylases are found in organisms across the evolutionary spectrum. The biotin carboxyl carrier domains of proteins from organisms ranging from bacteria to humans exhibit a high level of sequence homology (Samols et al., 1988), and cross-species biotin ligation has been demonstrated in several systems. For example, Cronan and co-workers have shown that the *E. coli* biotin ligase can catalyze modification of BCC domains from sources ranging from bacteria to tomato in vivo (Cronan, 1990). Gravel and co-workers demonstrated, moreover, that the biotin ligase from humans can rescue a temperature-sensitive mutation in the *E. coli* enzyme in vivo (Leon-Del-Rio et al., 1995). This functional and sequence conservation undoubtedly reflects structural conservation, and the availability of the three-dimensional structure of the *E. coli* apoBCCP will serve as a model for understanding the specific biotin ligation reaction in all organisms.

ACKNOWLEDGMENT

We are grateful to Dr. M. Zawrotny and R. Edwards (UMBC, Howard Hughes Medical Institute) for technical support.

SUPPORTING INFORMATION AVAILABLE

Two tables, summarizing the chemical shifts of apoBCCP87 and the analysis of dynamical data (10 pages). Ordering information is given on any current masthead page.

REFERENCES

Alberts, A. W., & Vagelos, P. R. (1972). Acyl-CoA Carboxylases, in *The Enzymes* (Boyer, P. D., Ed.) Vol. 6, pp 37−82, Academic Press, Orlando, FL.

Athappilly, F. K., & Hendrickson, W. A. (1995) Structure of the biotinyl domain of acetyl-coenzyme A carboxylase determined by MAD phasing, *Structure 3*, 1407−1419.

Bacon, D. J., & Anderson, W. F. (1988) A fast algorithm for rendering space-filling molecule pictures, *J. Mol. Graphics 6*, 219−220.

Bax, A., Ikura, M., Kay, L. E., & Zhu, G. (1991) Removal of *F*1 baseline distortion and optimization of folding in multidimensional NMR spectra, *J. Magn. Reson. 91*, 174−178.

Barbato, G., Ikura, M., Kay, L. E., Pastor, R. W., & Bax, A. (1992) Backbone dynamics of calmodulin studied by ^{15}N relaxation using inverse detected two-dimensional NMR spectroscopy: the central helix is flexible, *Biochemistry 31*, 5269−5278.

Brocklehurst, S. M., & Perham, R. N. (1993) Prediction of the Three-Dimensional Structures of the Biotinylated Domain from Yeast Pyruvate Carboxylase and of the Lipoated H-protein of the Pea Leaf Glycine Cleavage System: A New Automated Method for the Prediction of Protein Tertiary Structure, *Protein Sci. 2*, 626−639.

Bothner-by, A., Stephens, R. L., Lee, J.-m., Warren, C. D., & Jeanloz, R. W. (1984) Structure determination of a tetrasaccharide: Transient nuclear Overhauser effects in the rotating frame, *J. Am. Chem. Soc. 106*, 811−813.

Carr, H. Y., & Purcell, E. M. (1954) Effects of diffusion on free precession in nuclear magnetic resonance experiments, *Phys. Rev. 4*, 630−638.

Clore, G. M., Gronenborn, A. M., Nilges, M., & Ryan, C. A. (1987) Three-dimensional structure of potato carboxypeptidase inhibitor in solution. A study using nuclear magnetic resonance, distance geometry, and restrained molecular dynamics, *Biochemistry 26*, 8012−8023.

Cronan, J. E., Jr., (1990) Biotination of Proteins in Vivo, *J. Biol. Chem. 265*, 10327−10333.

Dardel, F., Laue, E. D., & Perham, R. N. (1991) Sequence-cspecific ^{1}H-NMR Assignments and Secondary Structure of the Lipoyl Domain of the *Bacillus stearothermophilus* Pyruvate Dehydrogenase Multienzyme Complex, *Eur. J. Biochem. 201*, 203−209.

Dardel, F., Davis, A. L., Laue, E. D., & Perham, R. N. (1993) Three-Dimensional Structure of the Lipoyl Domain from *Bacillus stearothermophilus* Pyruvate Dehydrogenase Multienzyme Complex, *J. Mol. Biol. 229*, 1037−1048.

Dimroth, P., Guchait, R. B., Stoll, E., & Lane, M. D. (1970) Enzymatic Carboxylation of Biotin: Molecular and Catalytic Properties of a Component Enzyme of Acetyl-CoA Carboxylase, *Proc. Natl. Acad. Sci. U.S.A. 67*, 1353−1360.

Fall, R. R. (1979) Analysis of Microbial Biotin Proteins, *Methods Enzymol. 62*, 390−398.

Farrow, N. A., Muhandiram, R., Singer, A. U., Pascal, S. M., Kay, C. M., Gish, G., Shoelson, S. E., Pawson, T., Forman-Kay, J. D., & Kay, L. E. (1994) Backbone dynamics of a free and a phosphopeptide-complexed Src homology 2 domain studied by ^{15}N NMR relaxation, *Biochemistry 33*, 5984−6003.

Green, J. D. F. , Laue, E. D., Perham, R. N., Ali, S. T., & Guest, J. R. (1995) Three-Dimensional Structure of a Lipoyl Domain from the Dihydrolipoyl Acetyltransferase Component of the Pyruvate Dehydrogenase Multienzyme Complex of *Escherichia coli*, *J. Mol. Biol. 248*, 328−343.

Griesinger, C., Otting, G., Wüthrich, K., & Ernst, R. R. (1988) Clean TOCSY for ^{1}H spin system identification in macromolecules, *J. Am. Chem. Soc. 110*, 7870−7872.

Grzesiek, S., & Bax, A. (1993) The Importance of Not Saturating H_2O in Protein NMR. Application to Sensitivity Enhancement and NOE Measurement, *J. Am. Chem. Soc. 115*, 12593−12593.

Guchhait, R. B., Polakis, S. E., Dimroth, P., Stoll, E., Moss, J., & Lane, M. D., (1974) Acetyl Coenzyme A Carboxylase System of *Escherichia coli*: Purification and Properties of the Biotin Carboxylase, Carboxyltransferase, and Carboxyl Carrier Protein Components, *J. Biol. Chem. 249*, 6633−6645.

Güntert, P., & Wüthrich, K. (1991) Improved Efficiency of Protein Structure Calculations from NMR Data Using the Program DIANA with Redundant Dihedral Angle Constraints, *J. Biomol. NMR 1*, 447−456.

Güntert, P., Braun, W., & Wüthrich, K. (1991) Efficient computation of three-dimensional protein structures in solution from nuclear magnetic resonance data using the program DIANA and the supporting programs CALIBA, HABAS and GLOMSA, *J. Mol. Biol. 217*, 517−530.

Johnson, B. A., & Blevins, R. A. (1994) NMRview: a computer program for the visualization and analysis for NMR data, *J. Biomol. NMR 4*, 603−614.

Kay, L. E., Marion, D., & Bax, A. (1989a) Practical aspects of 3D heteronuclear NMR of proteins, *J. Magn. Reson. 84*, 72−84.

Kay, L. E., Torchia, D. A., & Bax, A. (1989b) Backbone dynamics of proteins as studied by ^{15}N inverse detected heteronuclear NMR spectroscopy: Application to staphylococcal nuclease, *Biochemistry 28*, 8972−8979.

Kay, L. E., Nicholson, L. K., Delaglio, F., Bax, A., & Torchia, D. A. (1992) Pulse sequences for the removal of the effects of cross correlation between dipolar and chemical-shift anisotropy relaxation mechanisms on the measurement of heteronuclear T_1 and T_2 values in proteins, *J. Magn. Reson. 97*, 359−375.

Knowles, J. R. (1989) The mechanism of biotin-dependent enzymes, *Annu. Rev. Biochem. 58*, 195−221.

Kraulis, P. J. (1991) MOLSCRIPT: a program to produce both detailed and schematic plots of protein structures, *J. Appl. Crystallogr. 24*, 946−950.

Lane, M. D., Rominger, K. L., Young, D. L., & Lynen, F. (1964) The Enzymatic Synthesis of Holotranscarboxylase from Apotranscarboxylase and (+)-Biotin, *J. Biol. Chem. 239*, 2865−2871.

Laskowski, R. A., MacArthur, M. W., Moss, D. S., & Thornton, J. W. (1993) PROCHECK: a program to check the stereochemical quality of protein structures, *J. Appl. Crystallogr. 26*, 283−291.

Leon-Del-Rio, A., Leclerc, D., Akerman, B., Wakamatsu, N., & Gravel, R. A. (1995) Isolation of a cDNA Encoding Human Holocarboxylase Synthetase by Functional Complementation of a Biotin Auxotroph of *Escherichia coli*, *Proc. Natl. Acad. Sci. U.S.A. 92*, 4226−4230.

Li, S.-J., & Cronan, J. E., Jr. (1992a) The Gene Encoding the Biotin Carboxylase Subunit of *Escherichia coli* Acetyl-CoA Carboxylase, *J. Biol. Chem. 267*, 855−863.

Li, S.-J., & Cronan, J. E., Jr. (1992b) The Genes Encoding the Two Carboxyltransferase Subunits of *Escherichia coli* Acetyl-CoA Carboxylase, *J. Biol. Chem. 267*, 16841−16847.

Lim, F., Morris, C. P., Occhiodoro, F., & Wallace, J. C. (1988) Sequence and Domain Structure of Yeast Pyruvate Carboxylase, *J. Biol. Chem. 263*, 11493−11497.

Lipari, G., & Szabo, A. (1982) Model-free approach to the interpretation of nuclear magnetic resonance relaxation in macromolecules. 1. Theory and range of validity, *J. Am. Chem. Soc. 104*, 4546−4559.

Mandel, A. M., Mikael, A., & Palmer, A. G. (1995) Backbone dynamics of *Escherichia coli* Ribonuclease HI: correlations with structure and function in an active enzyme, *J. Mol. Biol. 246*, 144−163.

Marion, D., & Bax, A. (1989) Baseline correction of 2D FT NMR spectra using a simple linear prediction extrapolation of the time-domain data, *J. Magn. Reson. 83*, 205−211.

Marion, D., Kay, L. E., Sparks, S. W., Torchia, D. A., & Bax, A. (1989a) Three-dimensional heteronuclear NMR of ^{15}N-labeled proteins, *J. Am. Chem. Soc. 111*, 1515−1517.

Marion, D., Driscoll, P. C., Kay, L. E., Wingfield, P. T., Bax, A., Gronenborn, A. M., & Clore, G. M. (1989b) Overcoming the overlap problem in the assignment of ^{1}H NMR spectra of larger proteins by use of three-dimensional heteronuclear ^{1}H-^{15}N Hartmann−Hahn−multiple quantum coherence and nuclear Overhauser−multiple quantum coherence spectroscopy: application to interleukin 1b, *Biochemistry 28*, 6150−6156.

Marion, D., Ikura, M., Tschudin, R., & Bax, A. (1989c) Rapid recording of 2D NMR spectra without phase cycling. Application to the study of hydrogen exchange in proteins, *J. Magn. Reson. 85*, 393−399.

Meiboom, S., & Gill, D. (1958) Modified spin−echo method for measuring nuclear spin relaxation times, *Rev. Sci. Instrum. 29*, 688−691.

Nenortas, E., & Beckett, D. (1996) Purification and characterization of intact and truncated forms of the *Escherichia coli* biotin carboxyl carrier subunit of acetyl-CoA carboxylase, *J. Biol. Chem. 271*, 7559−7567.

Noggle, J. H., & Shirmer, R. E. (1971) *The Nuclear Overhauser Effect: Chemical Applications*, pp 1−259, Academic Press, New York.

Palmer, A. G., Rance, M., & Wright, P. E. (1991) Intramolecular motions of a zinc finger DNA-binding domain from xfin characterized by proton-detected natural abundance ^{13}C heteronuclear NMR spectroscopy, *J. Am. Chem. Soc 113*, 4371−4380.

Pares, S., Cohen-Addad, C., Sieker, L., Neuburger, M., & Douce, R. (1994) X-ray Structure Determination at 2.6-Å Resolution of a Lipoate-Containing Protein: The H-protein of the Glycine Decarboxylase Complex from Pea Leaves, *Proc. Natl. Acad. Sci. U.S.A. 91*, 4850−4853.

Peng, J. W., & Wagner, G. (1992) Mapping of spectral density functions using heteronuclear NMR relaxation measurements, *J. Magn. Reson. 98*, 308−332.

Piotto, M., Saudek, V., & Sklenar, V. (1992) Gradient-tailored excitation for single-quantum NMR spectroscopy of aqueous solutions, *J. Biomol. NMR 2*, 661−665.

Press, W. H., Teukolsky, S. A., Vetterling, W. T., & Flannery, B. P. (1992) Numerical recipes in C: the art of scientific computing, pp 317−323, Cambridge University Press, Cambridge, U.K.

Rance, M., Sørensen, O. W., Bodenhausen, G., Wagner, G., Ernst, R. R., & Wüthrich, K. (1983) Improved spectral resolution in COSY ^{1}H NMR spectra of proteins via double quantum filtering, *Biochem. Biophys. Res. Commun. 117*, 479−485.

Samols, D., Thornton, C. G., Murtif, V. L., Kumar, G. K., Haase, F. C., & Wood, H. G. (1988) Evolutionary Conservation Among Biotin Enzymes, *J. Biol. Chem. 263*, 6461−6464.

Shaka, A. J., Keler, J., & Freeman, R. (1983) Evaluation of a new broadband decoupling sequence: WALTZ-16, *J. Magn. Reson. 53*, 313−340.

Spera, S., Ikura, M., & Bax, A. (1991) Measurement of the exchange rates of rapidly exchanging amide protons: application to the study of calmodulin and its complex with myosin light chain kinase fragment, *J. Biomol. NMR 1*, 155−165.

Tjandra, N., Feller, S. E., Pastor, R. W., & Bax, A. (1995) Rotational diffusion anisotropy of human ubiquitin from ^{15}N NMR relaxation, *J. Am. Chem. Soc. 117*, 12562−12566.

Tjandra, N., Wingfield, P., Stahl, S., & Bax, A. (1996) Anisotropic rotational diffusion of perdeuterated HIV protease from ^{15}N NMR relaxation measurements at two magnetic fields, *J. Biomol. NMR 8*, 273−284.

Vold, R. L., Waugh, J. S., Klein, M. P., & Phelps, D. E. (1968) Measurement of spin relaxation in complex systems, *J. Chem. Phys. 48*, 3831−3832.

Waldrop, G. L., Rayment, I., & Holden, H. M. (1994) Three-dimensional structure of the biotin carboxylase subunit of acetyl-CoA carboxylase, *Biochemistry 33*, 10249−10256.

Wilson, K. P., Shewchuk, L. M., Brennan, R. G., Otsuka, A. J., & Matthews, B. W. (1992) *Escherichia coli* biotin holoenzyme synthetase/bio repressor crystal structure delineates the biotin and DNA binding domains, *Proc. Natl. Acad. Sci. U.S.A. 89*, 9257−9261.

Wishart, D. S., Sykes, B. D., & Richards, F. M. (1991) Relationship between nuclear magnetic resonance chemical shift and protein secondary structure, *J. Mol. Biol. 222*, 311−333.

Wishart, D. S., Sykes, B. D., & Richards, F. M. (1992) The chemical shift index: a fast and simple method for the assignment of protein secondary structure through NMR spectroscopy, *Biochemistry 31*, 1647−1651.

Wüthrich, K. (1986) *NMR of Proteins and Nucleic Acids*, John Wiley & Sons, New York.

Zhang, O., Kay, L. E. Olivier, J. P., & Forman-Kay, J. D. (1994) Backbone ^{1}H and ^{15}N resonance assignments of the N-terminal SH3 domain of drk in folded and unfolded states using enhanced-sensitivity pulsed field gradient NMR techniques, *J. Biomol. NMR 4*, 845−858.

Zhu, G., Torchia, D. A., & Bax, A. (1993) Discrete Fourier transformation of NMR signals. The relationship between sampling delay time and spectral baseline, *J. Magn. Reson., Ser. A 105*, 219−222.

BI971485F